Supplement of The Cryosphere, 17, 3083–3099, 2023
https://doi.org/10.5194/tc-17-3083-2023-supplement

The Cryosphere Open Access EGU

Supplement of

Effects of extreme melt events on ice flow and sea level rise of the Greenland Ice Sheet

Johanna Beckmann and Ricarda Winkelmann

Correspondence to: Johanna Beckmann (johanna.beckmann@monash.edu)

S1 Initial state and comparison to present day

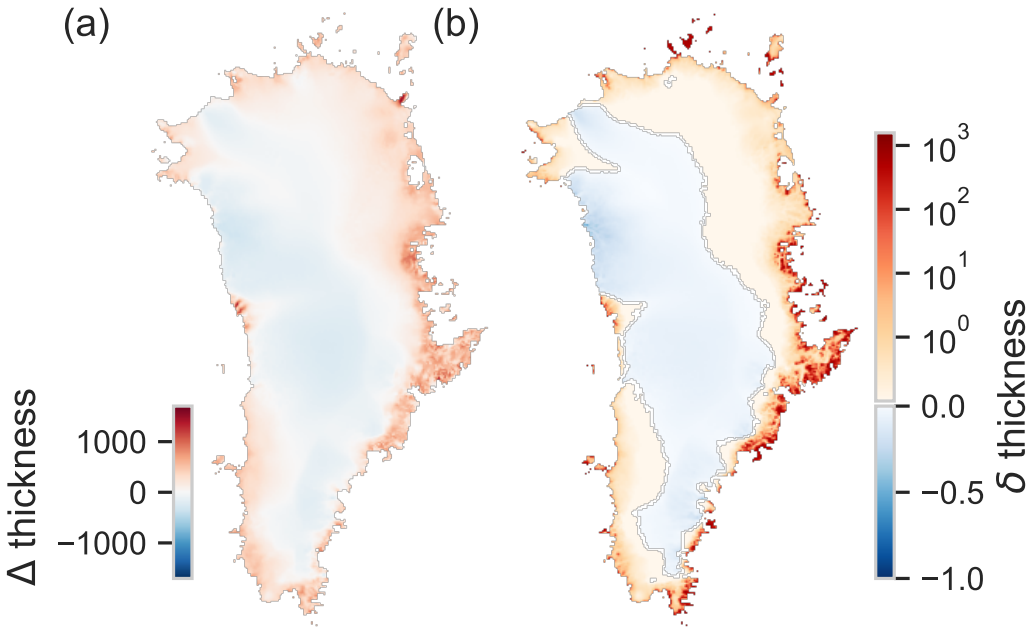

Fig. S1. Thickness anomalies between modelled initial state and observations. Given are **a** the ice thickness differences between the modelled initial state after a glacial cycle and observations (spinup -observation), with a RMSE of 237.92 metres and **b** the relative thickness difference to the observations with a RMSE of 93.78. Note that only fields with thicknesses above 1m were taken into account, as this was the original minimum thickness of the BedMachine version3 data Morlighem (2019). Blueish colors show where PISM underestimates thickness and reddish color show where PISM overestimates ice thickness.

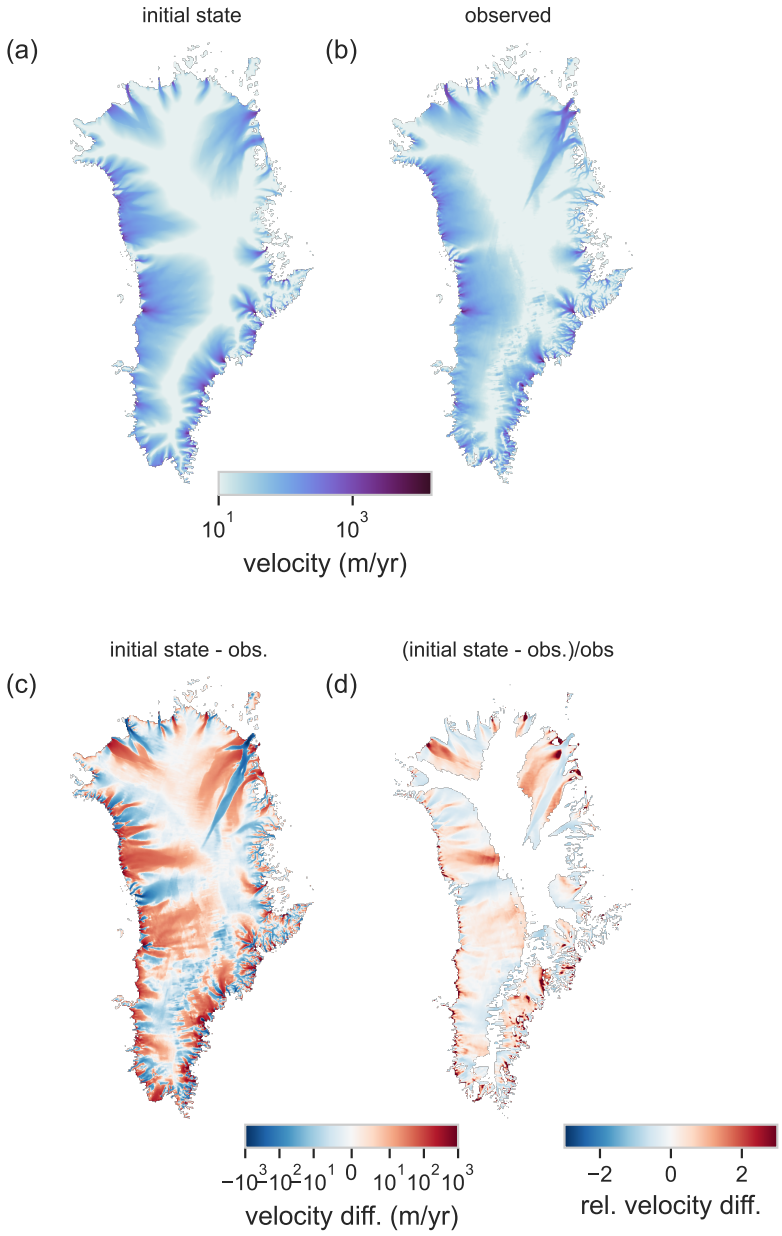

Fig. S2. Ice velocities. a Velocities of initial state and **b** the observed values (Joughin et al., 2018), averaged over years 1995-2015. **c** Differences between initial state and observations, with a RMSE of 146 m/yr for the entire ice sheet and of 413 m/yr for regions flowing faster than 100m/yr. **d** relative error to the observed velocity for regions of a minimum velocity of 10 ma^{-1}. Note that only velocity fields with thicknesses above 1m were taken into account, as this was the original minimum thickness of the BedMachine data Morlighem (2019).

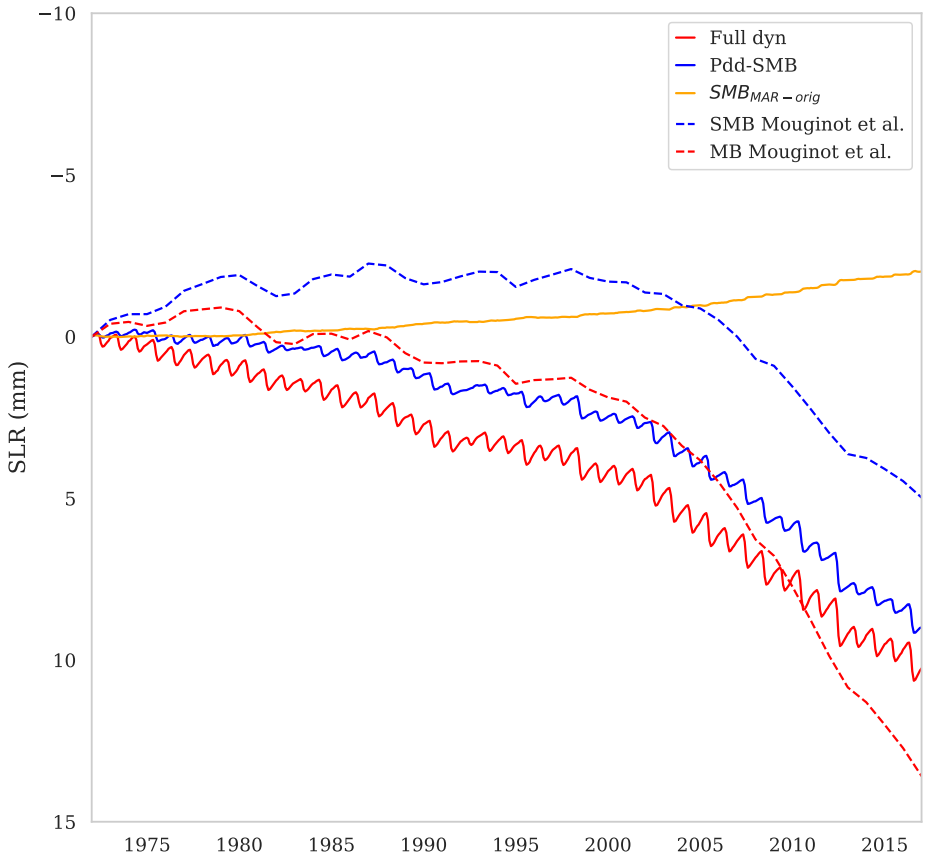

Fig. S3. Historical simulation(1972-2017) and observations. Given are the calculated SLR from PISM simulations full dynamic run in red and the cumulative SMB changes form the climatological mean from 1971-1999 calculated by the PISM-PDD model (blue) forced with the ERA-Temperature from 1972-2017. The full dynamic runs is subtracted by the control run (Fig. S15,SI) as our model is not in true balance but "observations" assume so. Observation Mouginot et al. (2019) from the cumulative SMB loss (blue dashed) were calculated by cumulative SMB anomalies of the SMB mean from 1961-1989 which wear taken from the Regional Atmospheric Climate Model v2.3p2 down scaled at 1km. The cumulative mass balance is depicted with the red dashed line. The cumulative SMB changes of climatological mean of 1971-1999 from the original MAR data give a sea level rise equivalent depicted in with the orange line.

S2 Temperature Forcing

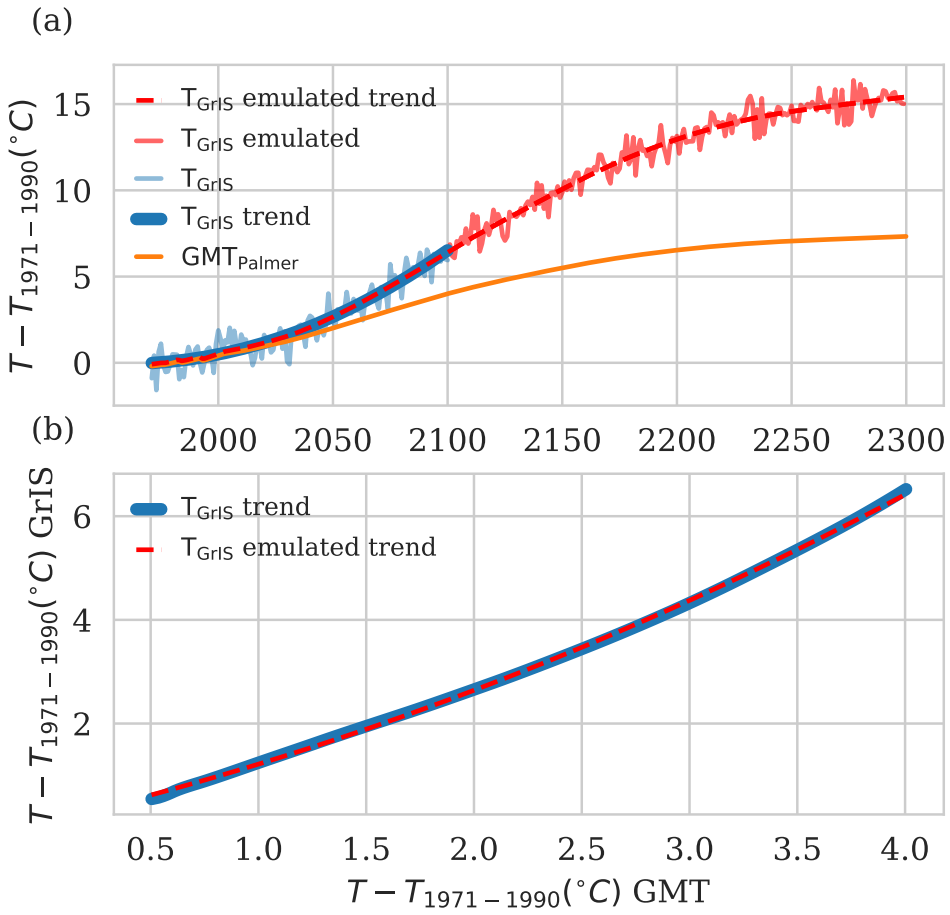

Fig. S4. Emulation of the annual average temperature anomaly over Greenland from 2100 to 2300. a Given is the emulated annual average temperature anomaly of Greenland (T_{GrIS} emulated; red solid line) and its trend (T_{GrIS} emulated trend; red dashed line) from 2100 until 2300, the annual temperature anomaly from MAR-MIROC5 (T_{GrIS}, blue solid line) and its derived quadratic trend (T_{GrIS} trend$= 1280.16^{\circ}C - 1.31^{\circ}C/year \cdot years + 20^{\circ}C/year^{-2} \cdot years^2$, blue thick line) from 1971 until 2100 as well as the global mean temperature from 1971 until 2300 emulated by Palmer et al. (2018) (orange line). **b** The temperature trend (T_{GrIS} trend, blue thick line) until 2100 and the global mean temperature until 2100 was used to derive an emulation function for the T_{GrIS} in dependence of the global mean temperature (GMT) with T_{GrIS} emulated trend$= 0.1^{\circ}C + 0.96^{\circ}C^{-1} \cdot GMT + 0.15^{\circ}C^{-2} \cdot GMT^2$ (red dashed line). This emulation function was then used to derive the emulated trend until year 2300 shown in **a**.

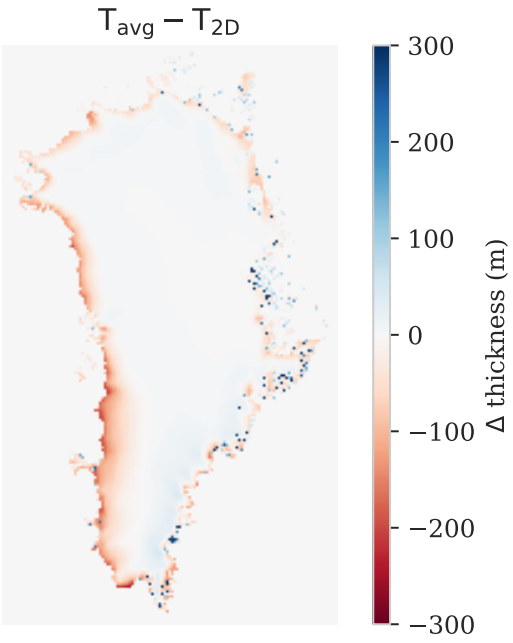

Fig. S5. Difference of ice thickness with pdd-simulations using a scalar temperature field and a spatial 2D temperature field at the year 2100. The reddish area shows where our ice loss simulation is overestimated compared to simulations with a 2D temperature field in the year 2100. Blueish area show the regions of underestimated mass loss.

S2.1 Evolution of extremes

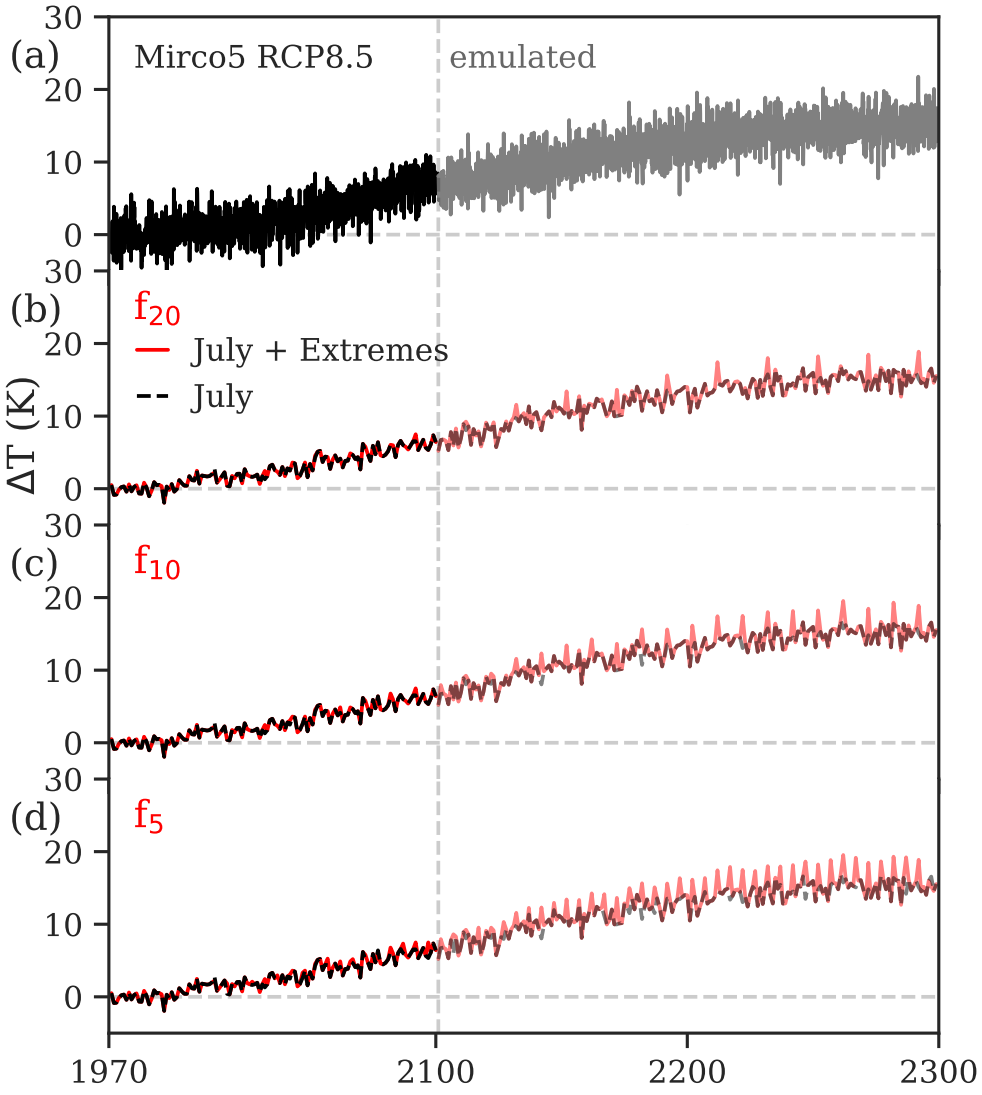

Fig. S6. Temperature scenarios $\mathbf{I}_{1.25}$ for the Greenland Ice Sheet. Given is the temperature anomaly over Greenland, based on the MIROC5 RCP8.5 projections, which is applied uniformly at the ice-sheet surface. **a** The forcing scenario without extremes on a monthly timescale (black, solid) from MIROC5 projection until year 2100, and emulated (grey) thereafter (see Methods). **b-d** July temperature projection (black, dashed) including extremes (red) occurring every 20 (f_{20}), 10 (f_{10}) and 5 (f_5) years with an intensity of 1.25 times the 10-year running mean ($I_{1.25}$).

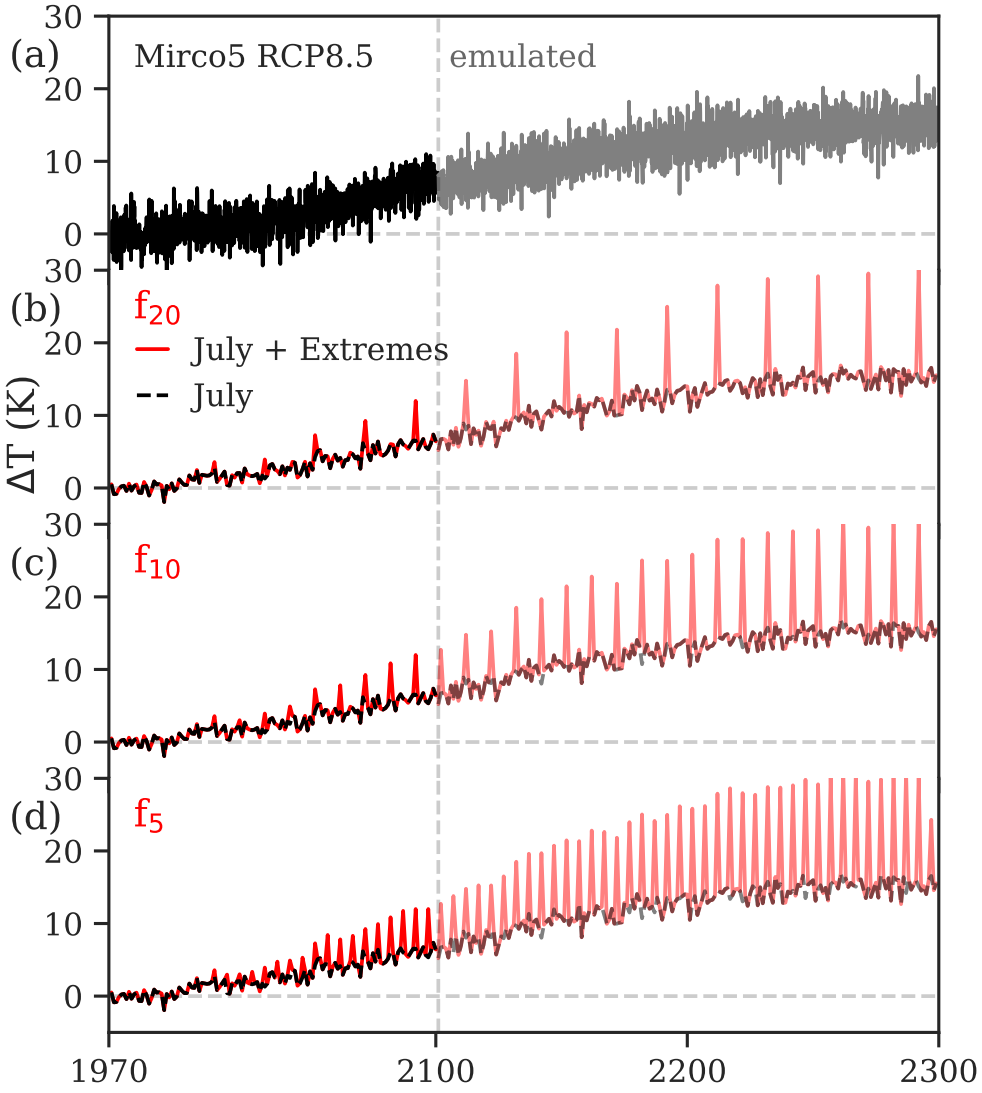

Fig. S7. Temperature scenarios I_2 for the Greenland Ice Sheet. Given is the temperature anomaly over Greenland, based on the MIROC5 RCP8.5 projections, which is applied uniformly at the ice-sheet surface. **a** The forcing scenario without extremes on a monthly timescale (black, solid) from MIROC5 projection until year 2100, and emulated (grey) thereafter (see Methods). **b-d** July temperature projection (black, dashed) including extremes (red) occurring every 20 (f_{20}), 10 (f_{10}) and 5 (f_5) years with an intensity of 2 times the 10-year running mean (I_2).

Based on our knowledge of the past temperature distribution including the respective frequencies of extremes ($\mathrm{f_{old}}$) and temperature levels reached during an extreme event ($\mathrm{T_{old}}$)), we can put future extremes occurring in generally warmer climates into context:

The temperature distribution can either shift to higher temperatures or the variance can broaden or the combination of the two might happen. All three cases lead to a higher frequency of the extreme temperatures observed in the old climate $\mathrm{f_{new}(T_{old})}$. Similarly this means that the extreme frequency of the old climate are now substituted by higher temperatures $\mathrm{f_{old}(T_{new})}$. How much these new extreme temperatures might actually increase in future we can only speculate, but it is certain that with increased temperatures the intensity of the extremes will get higher, as the distribution shifts or broadens more and more. For simplicity, we therefore here use idealized scenarios, applying a factor of 1.25, 1.5 and 2 times to the 10-year running mean. Note that in our approach the 10-year running mean always refers to the baseline scenario and excludes potentially added extremes from the years before. Figures S5 and S6 show that the extremes would increase in a similar manner if we calculated them from the observed temperature distributions and standard deviation of the past years. For example, the 2012 July temperature was 2.6 standard deviations above the 1971-2011 mean. Considering new extremes with the same 2012-deviation, leads to a temperature increase comparable to our $\mathrm{I_{1.5}, f_5}$ scenario (Fig. S8). Similarly does this approach compare well with our $\mathrm{I_2, f_5}$ scenario if the temperature distribution of only the last 15 years is considered (Fig. S9). Note that in this case, every new extreme adds to the temperature distribution thereafter.

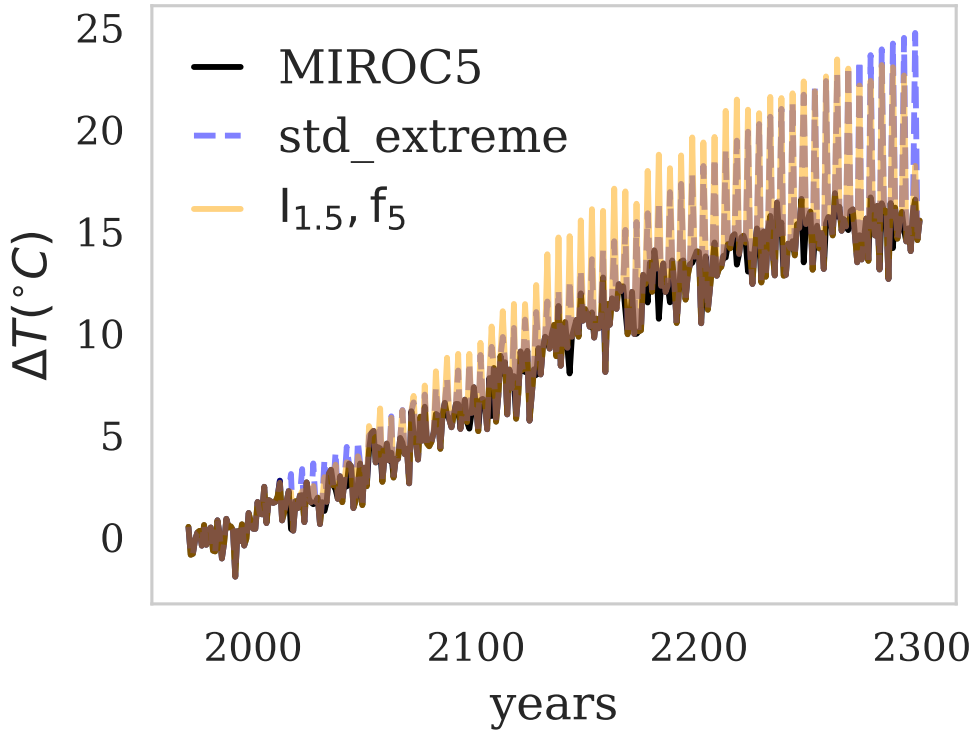

Fig. S8. Evolution of different extreme temperature scenarios from past temperature distribution. Given is the temperature anomaly over Greenland, based on the MIROC5 RCP8.5 projections (black) and the scenarios$\mathrm{I}_1.5, \mathrm{f}_5$ (yellow). Looking at the July temperature distribution from 1979 until 2011, the 2012 temperature was 2.6 standard deviations from the mean value away. Every 5 years the new extreme is created by looking at the past temperature distribution from 1979 to the current year and adding a extreme temperature that is 2.6 standard deviations away from the total mean ($\mathrm{std_e xtreme, bluedashed}$). Subsequent extreme calculations includes a temperature distribution that contains bygone extremes.

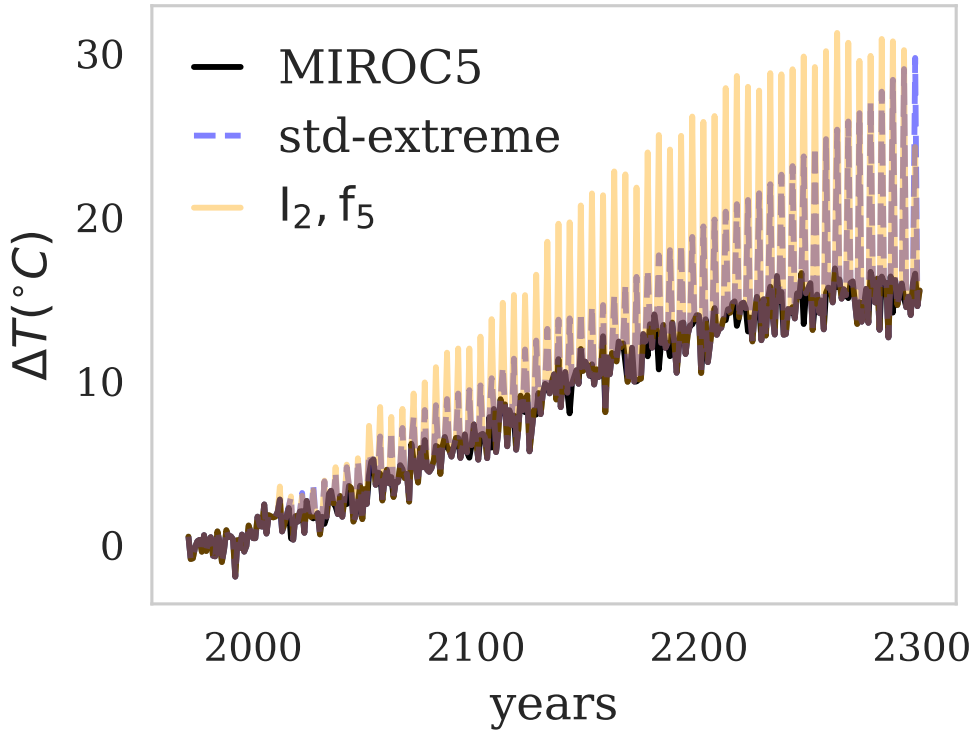

Fig. S9. Evolution of different extreme temperature scenario from 15-year temperature distribution . Given is the temperature anomaly over Greenland, based on the MIROC5 RCP8.5 projections (black) and the scenariosI_2, f_5 (yellow). Using the the last 15-years of July temperature gives that the 2012 extreme event was 2.2 standard deviation of the 1996-2011 histogram . Adding every 5 years an extreme with the same standard deviation of its past 15-year temperature distribution (thus including newly created extremes) leads to the blue dashed line (std-extreme).

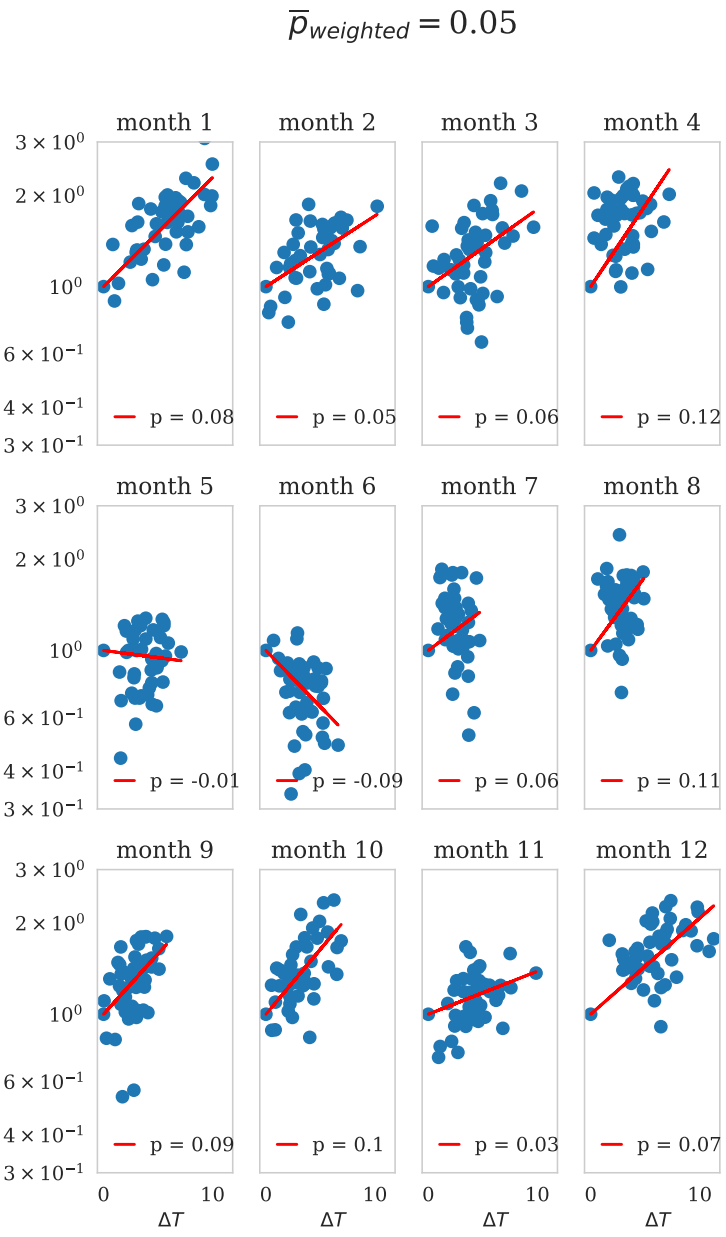

Fig. S10. Determination of precipitation factor p for the precipitation function $P = P_0 exp(p \cdot \Delta T)$ for the ERA Interim dataset. Each panel shows the monthly difference of precipitation P and the minimum precipitation at this month P_0 in 1971-2015 on a logarithmic scale and the temperature difference of $P - P_0$ (blue dots).The red line gives the determined monthly precipitation factor p. As a weighted sum they define the universal precipitation increase of 5% per degree of warming used in the experiments.

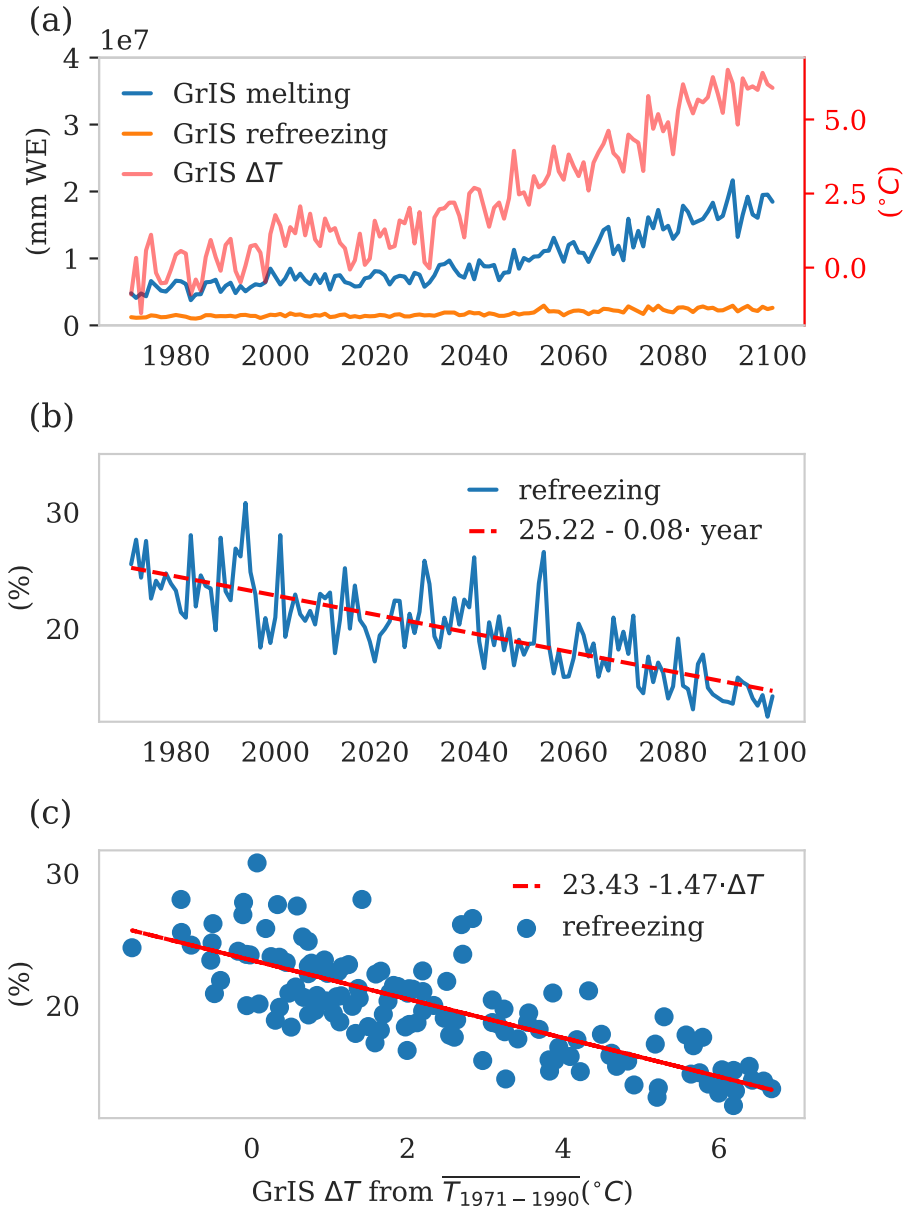

Fig. S11. Determination of refreezing parameter from the annual average surface temperature anomaly in Greenland. **a** Shown are the total melting (blue line), refreezing (orange line) and temperature over Greenland (reddish shading) over time for annual values, **b** the percentage of refreezing over time (blue line). The trend in time is given by $25.22\% - 0.08\%/year$ (red dashed line) with a p-values < 0.05 and a standard error of 0.005 %. **c** The temperature-dependent refreezing (blue points) determined with the percentage refreezing in **b** and the temperature anomaly in **a**. The red dashed line gives the temperature-dependent percentage refreezing function $(23.42 - 1.35 \cdot \Delta T)$ that has a p-value <0.05 and a standard error of 0.1

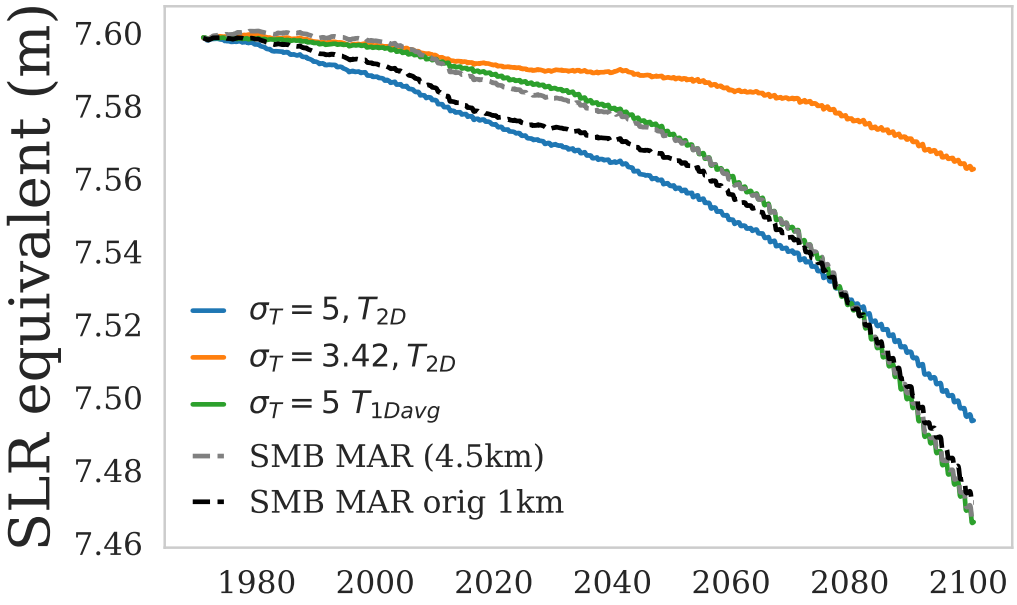

Fig. S12. Sea-level rise for different PDD parameters. Shown is the SLR calculated from a SMB-only scenario (without subtraction of the control run) with the temperature-dependent refreezing function determined in Fig. S11 for different constant standard deviations of 5 and 3.42. The orange and blue line show SMB calculations done with the 2D MAR temperature anomaly field, indicating the difficulty of modelling the SMB loss of MAR even when the same temperatures are used. Red lines shows SMB loss with a averaged scalar temperature field (as in our experimental setup).SLR from the original MAR data set (MAR-MIROC5) of 1km resolution was estimated by the cumulative changes in SMB over the entire ice sheet (also floating cells, SMB MAR orig 1km). The original data set was interpolated to our 4.5km grid as MAR (4.5km), where SLR was calculated by the cumulative changes of surface mass loss over over the volume above flotation (SMB MAR (4.5km),) in order to compare it correctly to the PISM PDD simulations.

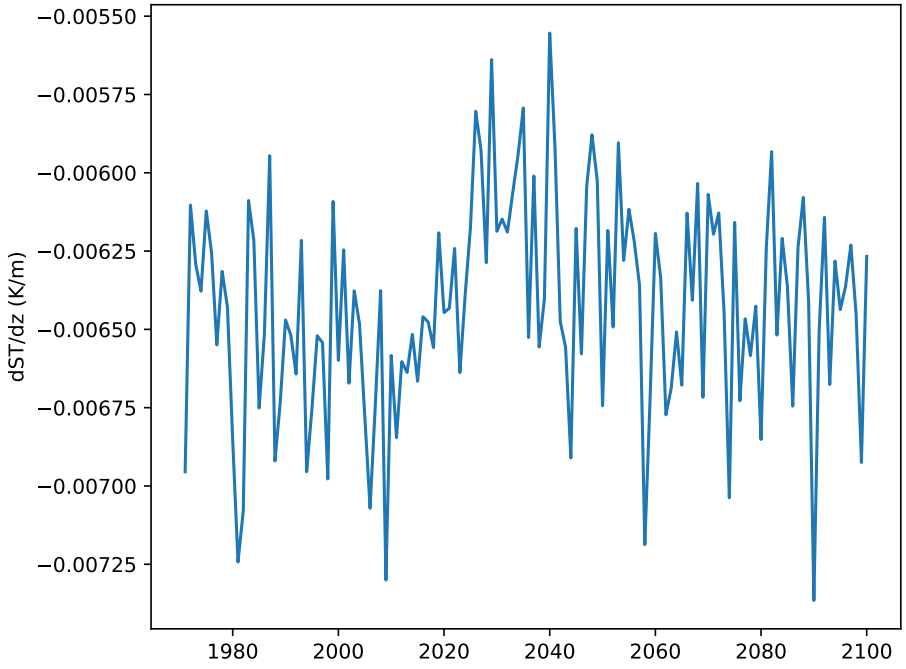

Fig. S13. Surface temperature gradient averaged over the GrIS. Temperature gradient was taken form the yearly MAR data sets for ERA and MIROC5.

S3 Sea level rise projections

All estimations of SLR always calculate the cumulative mass changes, that deviate from a state in balance. Observed SMB changes are calculated by regional climate Models that can determine melt, accumulation refreezing and surface run off etc. They calculate SMB loss and their cumulative change can be translated into SLR, because they assume the GrIS is in balance, and only changes in SMB would change SLR. These models do not consider dynamic changes.To simulate closely this surface mass loss form MAR with our PDD model, we therefore only consider the SMB changes simulated by the PDD model, therefore also assuming that our model is in balance. These are essentially our SMB only runs but are not subtracted by a model drift. This is only done to tune the PDD model to MAR SMB output in equivalent of SLR. However, the total observed mass balance loss is what in the end would give the true SLR. Because we know our model is not in balance (but the GrIS might gave been), we have to subtract the drift in order to compare SLR correctly. Therefore, whenever we compare our experiments with each other we subtract the model drift. Also , whenever we compare our simulations to “observations” that include dynamic changes.

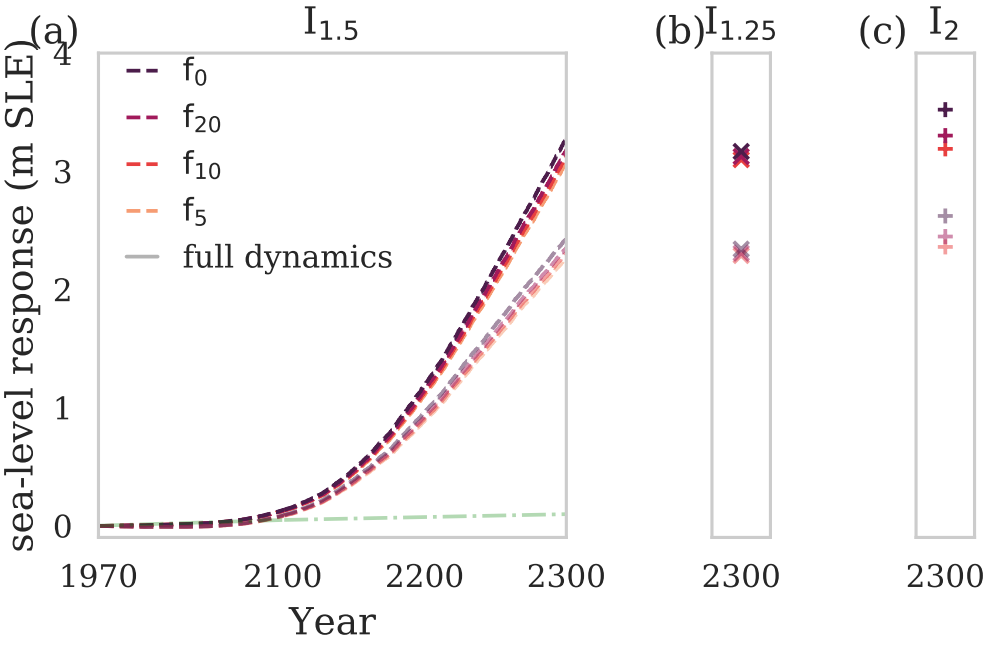

Fig. S14. Sea-level rise contribution of the Greenland Ice Sheet until 2300. **a** Fully dynamic sea-level rise contribution (dark colors) until 2300 for the forcing scenario without extremes (orange) and the extremes scenarios f_{20} (red), f_{10} (pink) and f_5 (purple) with intensity $I_{1.5}$. Light colors indicated the sea-level change due to SMB changes only.All run are subtracted by the control run (light green). **b,c** Sea level rise contribution for the same experiments but for lower and higher extreme event intensities of $I_{1.25}$ and I_5, respectively.

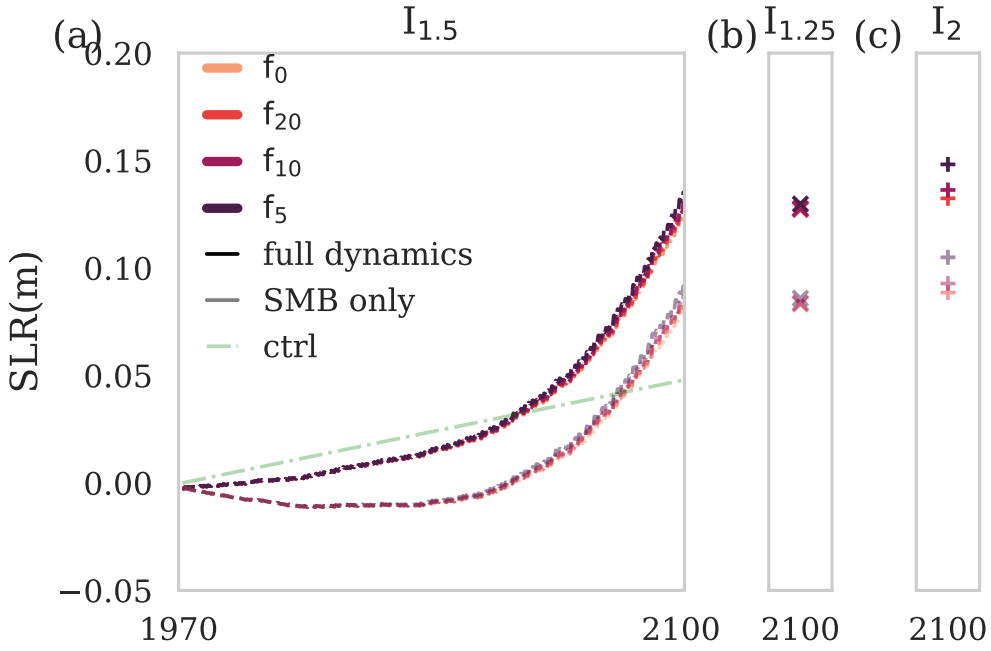

Fig. S15. Sea-level rise contribution of the Greenland Ice Sheet until 2100. **a** Fully dynamic sea-level rise contribution (dark colors) until 2100 for the forcing scenario without extremes (orange) and the extremes scenarios f_{20} (red), f_{10} (pink) and f_5 (purple) with intensity $I_{1.5}$. Light colors indicated the sea-level change due to SMB changes only.All run are subtracted by the control run (light green). **b,c** Sea level rise contribution for the same experiments but for lower and higher extreme event intensities of $I_{1.25}$ and I_5, respectively.

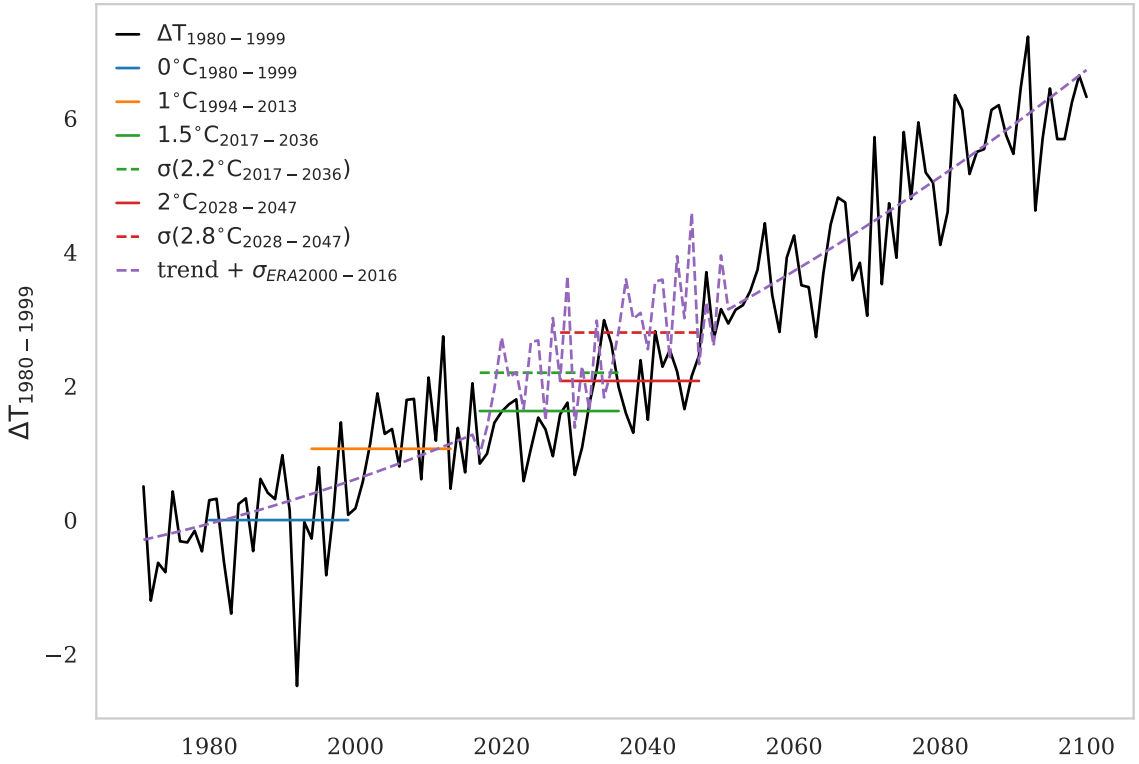

Fig. S16. Summer temperature anomalies to the mean of 1980-1999. Given is the summer (June-July-August) temperature anomaly to the mean of 1980-1999 in order to compare with Delhasse et al. (2018). The solid black lines give the summer temperature anomalies of our baseline scenario until 2100 ($\Delta T_{1980-1999}$), that included ERA Interim (until 2017) and MIROC5 after 2017. The solid colored horizontal give the time frame in which a mean temperature increase of $0°C_{1980-1990}$ (blue), $1°C_{1994-2014}$ (orange), $1.5°C_{2017-2037}$ (green) and $2°C_{2028-2048}$ (red) is achieved with our base line scenario. The purple dashed line depicts the trend of our baseline scenario plus the de-trended variability from 2000-2016 added for the time 2017- 2051 (trend + $\mathrm{sigma}_{\mathrm{ERA2000-2016}}$). Adding the summer variability of ERA from 2000-2016 would bring our experiments closer to the experiment of Delhasse et al. (2018) and would increase average temperature at least in the beginning of this century but not consider any increase in variability. By adding the summer ERA variability $\mathrm{sigma}_{\mathrm{ERA2000-2016}}$, the mean temperature of the baseline scenario of $1.5°C_{2017-2037}$ (green) and $2°C_{2028-2048}$ (red) would increase to $2.2°C$ ($\sigma(2.2°C_{2017-2037})$, green dashed) and $2.8°C$ ($\sigma(2.8°C_{2028-2048})$, red dashed) in the same time frames, respectively.

S4 Ice retreat and velocity changes

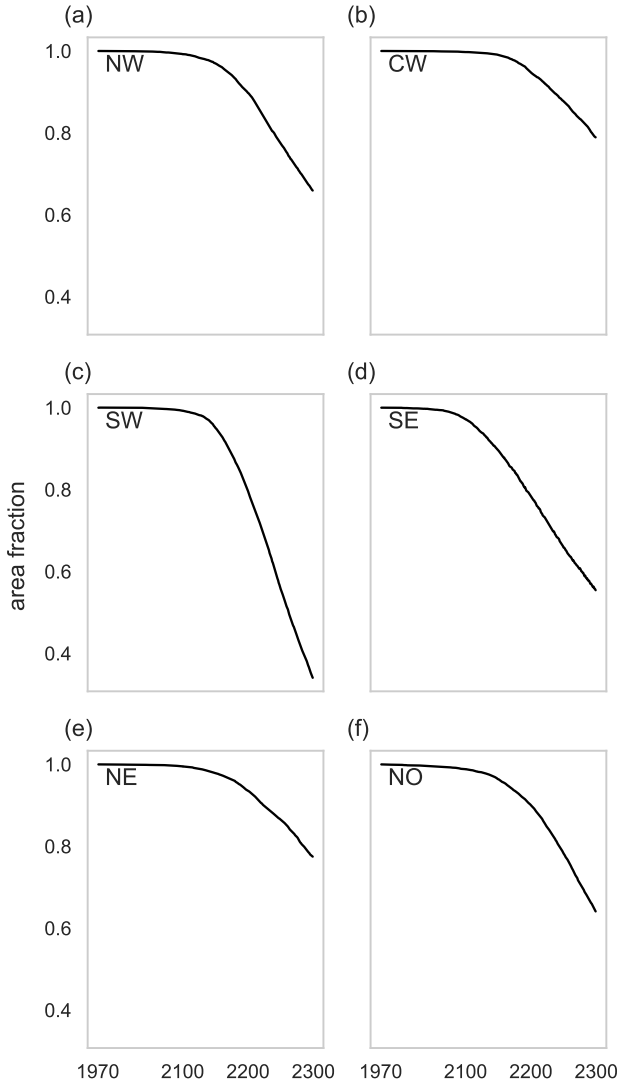

Fig. S17. Area fraction covered by the ice sheet $I_{1.5}, f_5$. Each panel shows the relative area covered by the ice sheet in respect to the year 1970 for each sector.

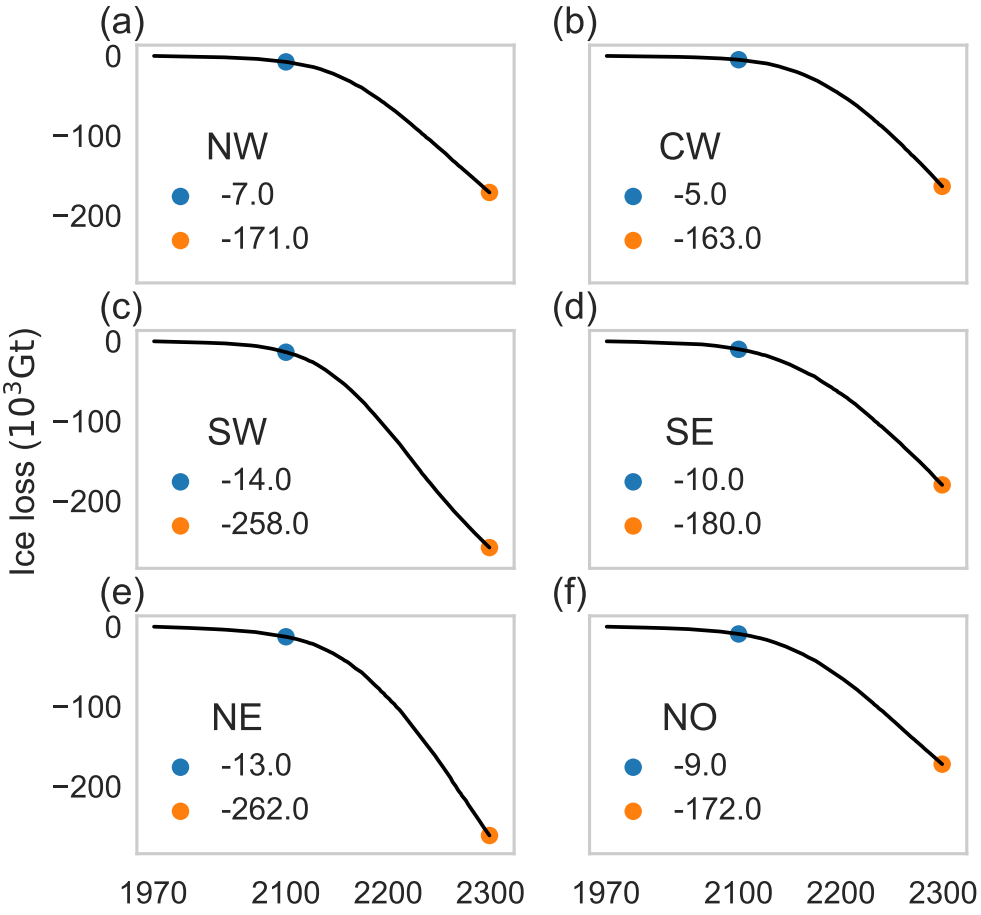

Fig. S18. Absolute ice loss from original ice volume for each sector for $I_{1.5}, f_5$. Each panel shows the ice volume changes over time for each sector. Given are the losses in the year 2100 (blue dot) and 2300 (orange dot). Note that only fields with thicknesses above 1m were taken into account, as this was the original minimum thickness of the BedMachine data Morlighem et al. (2017).

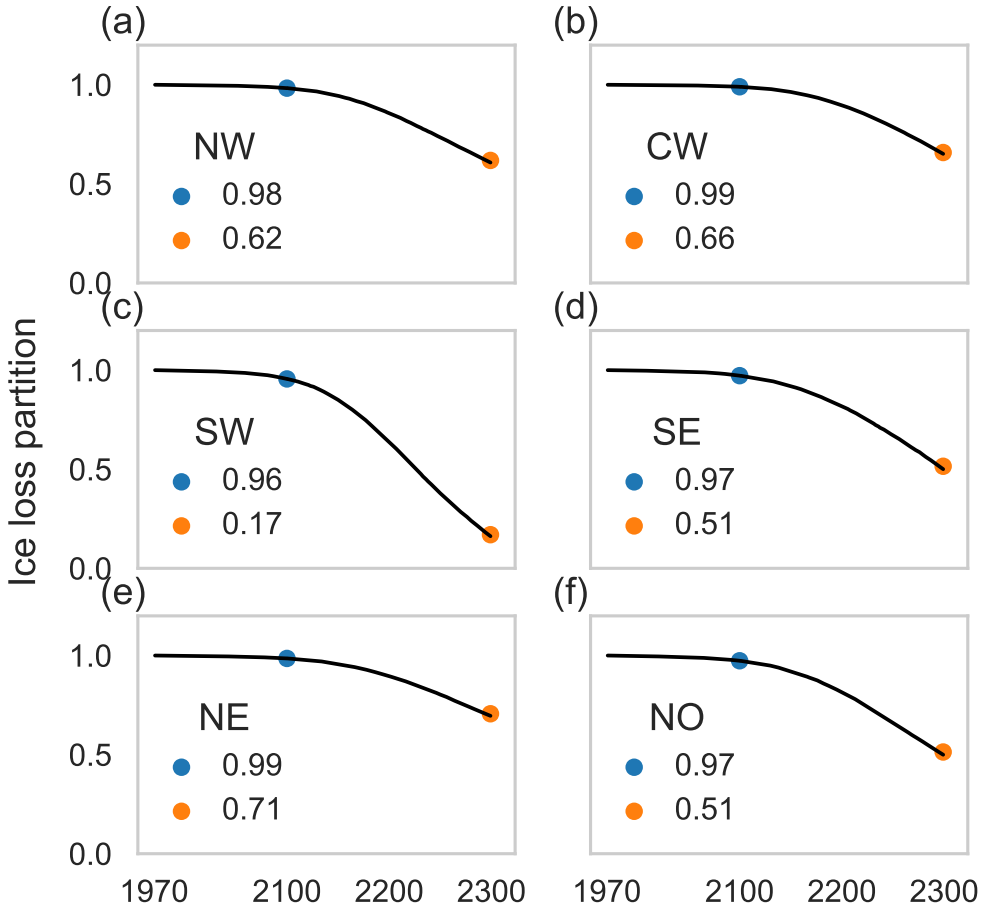

Fig. S19. Relative ice loss from original ice volume for each sector for $I_{1.5}, f_5$. Each panel shows the ice volume changes over time divided by its original ice volume in year 1970 for each sector. Given are the losses in the year 2100 (blue dot) and 2300 (orange dot). Note that only fields with thicknesses above 1m were taken into account, as this was the original minimum thickness of the BedMachine data Morlighem et al. (2017).

$I \backslash f$	Miroc5 (f=0)	f_{20}	f_{10}	f_5
1.25	652.84	655.67	659.28	665.58
1.50	652.84	659.30	666.97	679.69
2.00	652.84	667.30	681.76	710.82

Table S1. Ice area loss in 2300 for full dynamic runs. Given is the ice area loss in $10^3 \mathrm{km}^2$ for all intensity scenarios (I) and frequency ranges (f) for thicknesses greater than 1m of the full dynamic experiment compared to base the control run in 2300. The control run covered an area of 1795.12 $10^3 \mathrm{km}^2$ for ice thicknesses greater than 1m in 2300.

$I \backslash f$	Miroc5 (f=0)	f_{20}	f_{10}	f_5
1.25	0.0	2.84	6.44	12.74
1.50	0.0	6.46	14.13	26.85
2.00	0.0	14.46	28.92	57.98

Table S2. Ice area loss in 2300 compared to the baseline scenario of the full dynamic run. Given is the ice area loss in $10^3\mathrm{km}^2$ for all intensity scenarios (I) and frequency ranges (f) of the full dynamic experiment compared to base line scenario in 2300. The baseline scenario covered an area of 1142.28 $10^3\mathrm{km}^2$ for ice thicknesses greater than 1m in 2300.

$I \backslash f$	Miroc5 (f=0)	f_{20}	f_{10}	f_5
1.25	440.3	442.60	444.67	448.72
1.50	440.3	444.75	449.63	458.20
2.00	440.3	450.16	459.25	477.47

Table S3. Ice area loss in 2300 for dynamic runs without surface elevation feedback. Given is the ice area loss in $10^3\mathrm{km}^2$ for all intensity scenarios (I) and frequency ranges (f) of the full dynamic experiment compared to control run in 2300,which covered an area of 1795.12 $10^3\mathrm{km}^2$ for ice thicknesses greater than 1m.

$I \backslash f$	Miroc5 (f=0)	f_{20}	f_{10}	f_5
1.25	0.0	2.31	4.37	8.42
1.50	0.0	4.46	9.34	17.90
2.00	0.0	9.86	18.95	37.18

Table S4. Ice area loss in 2300 compared to the baseline scenario of the dynamic run without surface elevation feedback. Given is the ice area loss in $10^3\mathrm{km}^2$ for all intensity scenarios (I) and frequency ranges (f) of the full dynamic experiment compared to base line scenario in 2300. The baseline scenario covered an area of 1354.83 $10^3\mathrm{km}^2$ for ice thicknesses greater than 1m in 2300.

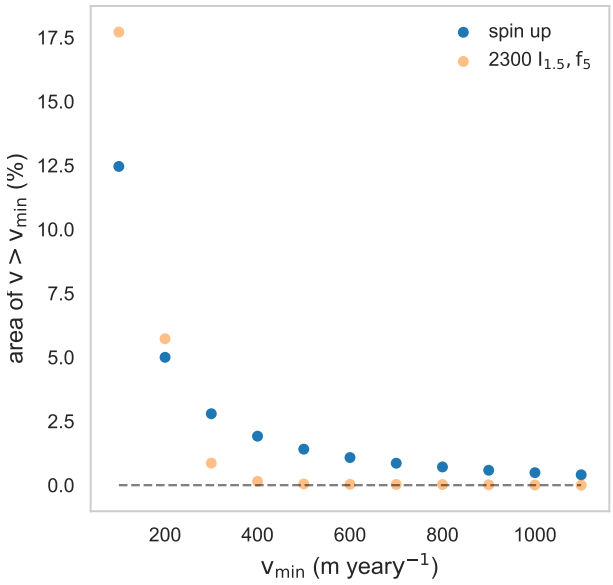

Fig. S20. Relative area with ice flowing with a certain minimum surface velocities. Area fraction is calculated from the ice sheet of the spin-up state (blue) the remaining ice sheet of the year 2300 for the extreme scenario $I_{1.5}, f_5$ in light orange in which ice flows with a certain minimum surface velocities. Note that only fields with thicknesses above 1m were taken into account, as this was the original minimum thickness of the BedMachine data Morlighem et al. (2017).

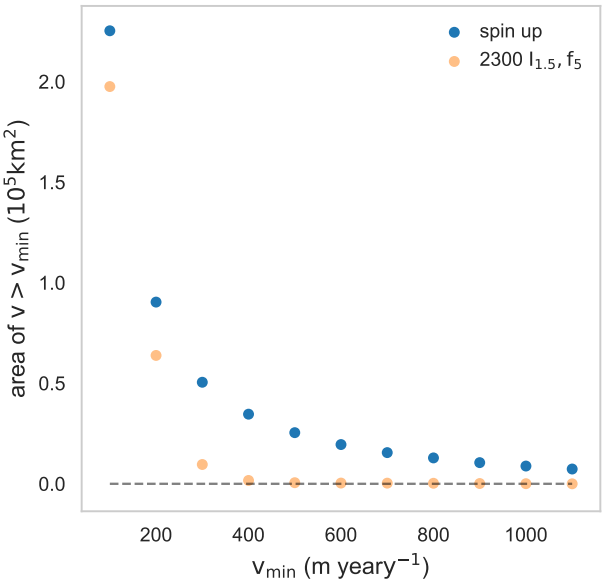

Fig. S21. Absolute area size where ice flows with a certain minimum surface velocities. Area is calculated from the ice sheet of the spin-up state (blue) the remaining ice sheet of the year 2300 for the extreme scenario $I_{1.5}, f_5$ in light orange in which ice flows with a certain minimum surface velocity. Note that only fields with thicknesses above 1m were taken into account, as this was the original minimum thickness of the BedMachine data Morlighem et al. (2017).

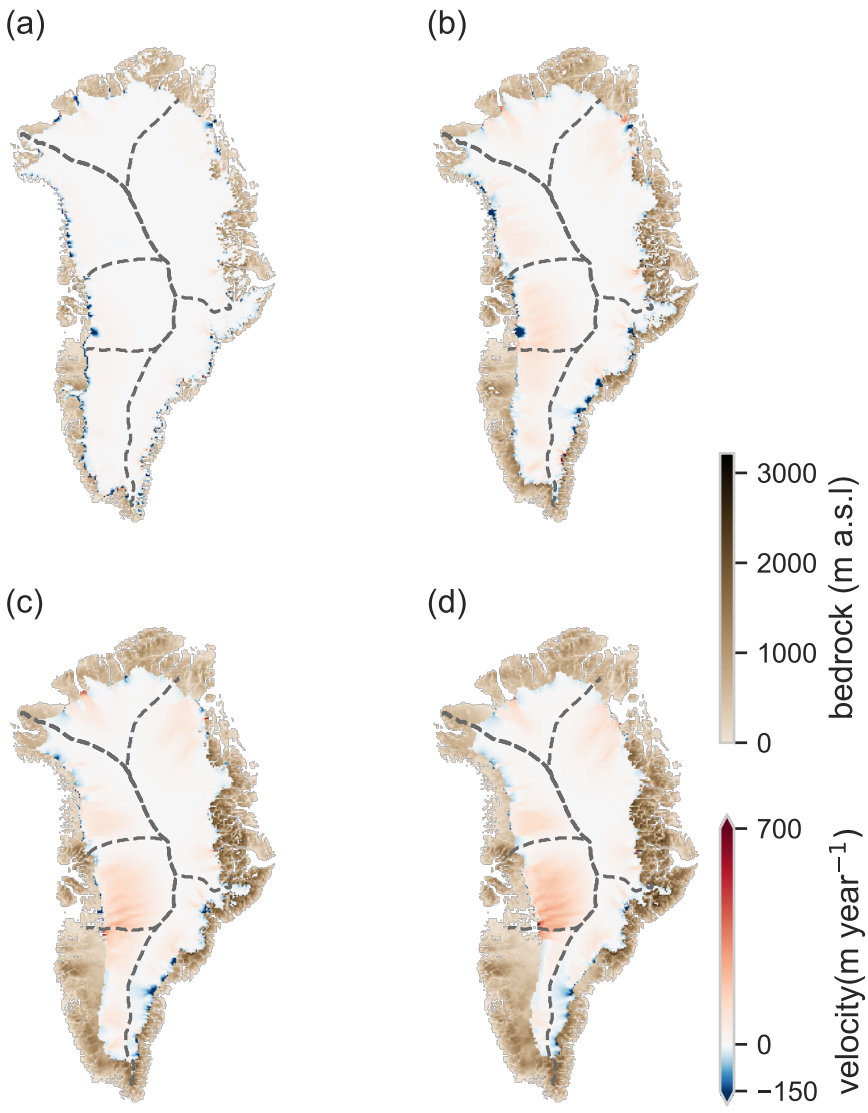

Fig. S22. Surface velocity difference of the $I_{1.5}, f_5$ scenario compared to the spin up velocities. For the remaining ice thickness the surface velocity field is subtracted by the surface velocity field of the spin-up state, for the year a)2100 b)2200 c)2250 and d) 2300 for the $I_{1.5}, f_5$ scenario. Reddish area means speedup while blueish area indicate slow down of the surface ice flow. Note that only fields with thicknesses above 1m were taken into account, as this was the original minimum thickness of the BedMachine data Morlighem et al. (2017).

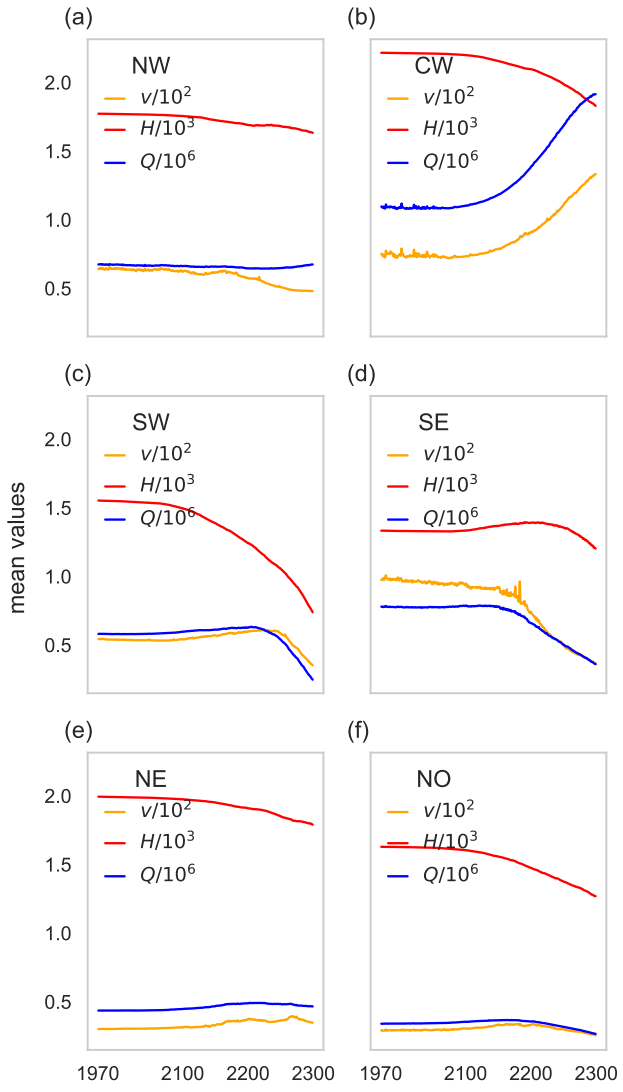

Fig. S23. Mean values of surface velocity (v), thickness (H) and flux (Q) for the $I_{1.5}, f_5$ scenario. Each panel hows the mean values of surface velocity (v in yellow), thickness (H in red) and flux (Q in blue) multiplied by a constant factor of 10^{-2} ,10^{-3} and 10^{-6}/190g respectively for each sector. The flux here is the mean vertically-integrated horizontal flux of each ice cell. Note that only fields with thicknesses above 1m were taken into account, as this was the original minimum thickness of the BedMachine data Morlighem et al. (2017).

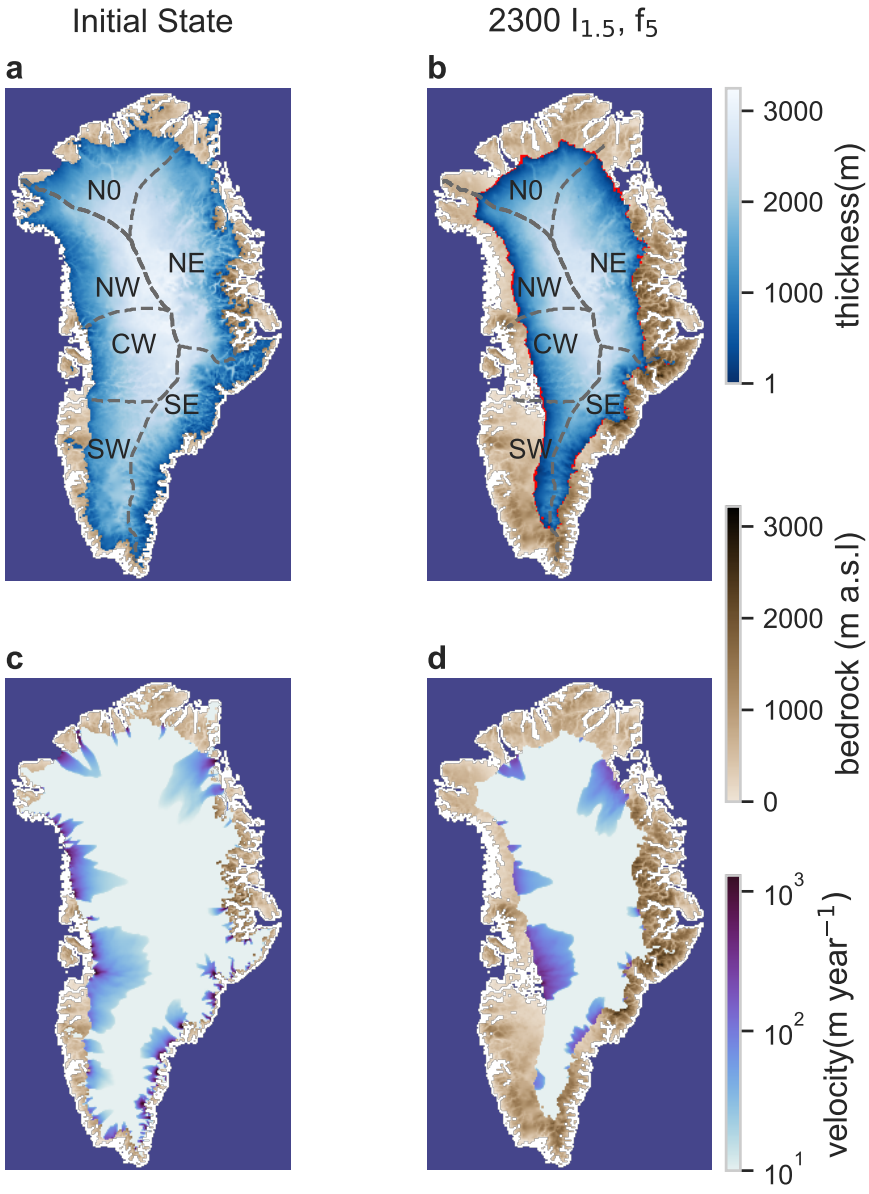

Fig. S24. Thickness basal velocities for spin-up and year 2300. (a) Ice thickness (in meters) of initial state with present-day boundary conditions and (c) the corresponding basal velocity field (in metres per year), as simulated with PISM. Basins are adjusted after (Rignot and Mouginot, 2012) by the IMBIE-2016 team (IMBIE2016, 2019). (b) Projected ice thickness distribution in the year 2300 under MIROC5 RCP8.5 temperature changes, including extreme events ($I_{1.5}, f_5$). Extremes are here applied by increasing the average temperature during the month of July by a factor of 1.5 every 5 years. Brown shading illustrates the bedrock elevation (in metres above sea-level). (d) Corresponding basal velocity field in the year 2300 based on the scenario $I_{1.5}, f_5$.

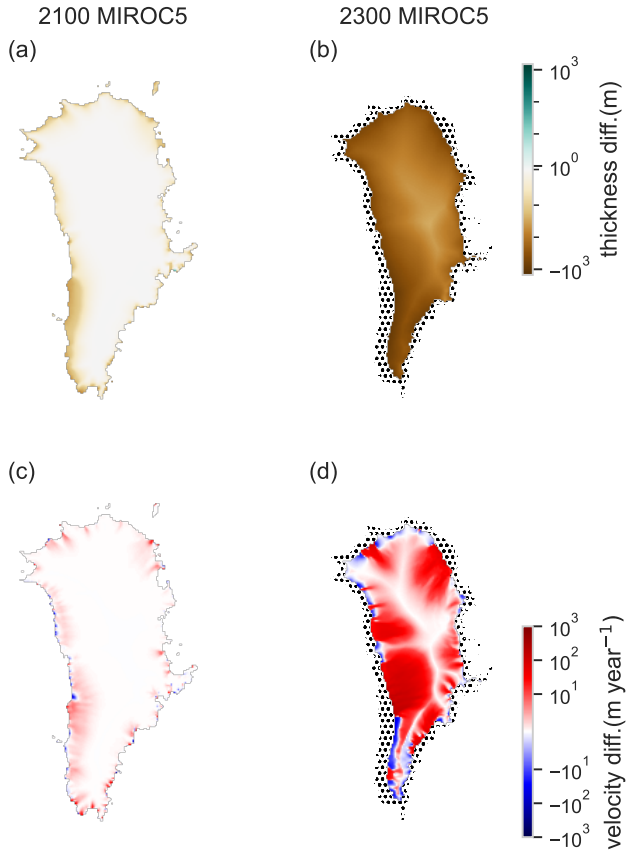

Fig. S25. Difference of dynamic runs with and without the surface elevation feedback. Shown is the difference (full dynamic run minus the dynamic runs without the surface elevation feedback) for the (a) thickness in the year 2100, (b) velocity in the year 2100 , (c) thickness in the year 2300 and (d) velocity in the year 2300 under the baseline scenario. Only the ice mask of the full dynamic run was considered. Extent of the ice mask of the dynamic run without surface elevation feedback is shown for the the dotted area. Brownish color in the thickness differences indicates where thinning is happening due to the surface elevation feedback. Reddish color in the velocity difference indicates where speedup is happening and blueish color where a slowdown is happening invoked by considering the surface elevation feedback.

S5 Role of intensity end frequency of extremes

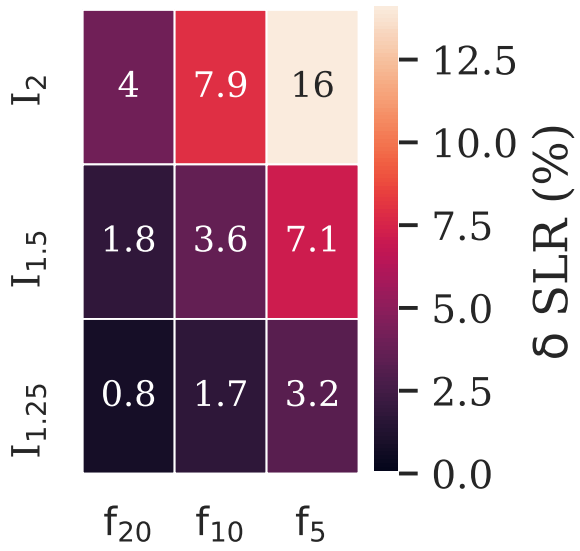

Fig. S26. Relative importance of intensity and frequency of extremes for the SMB only simulation. Given is the relative increase of the projected sea-level rise contribution in year 2300 of each extreme scenario to the scenario without extremes(MIROC5) for the SMB only case.

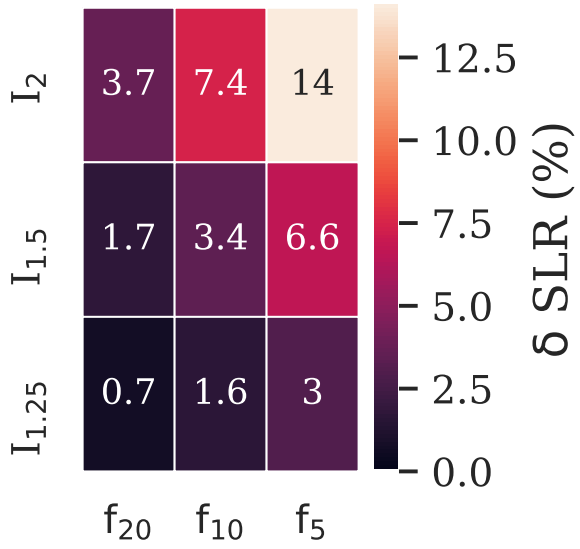

Fig. S27. Relative importance of intensity and frequency of extremes for the full dynamic simulation. Given is the relative increase of the projected sea-level rise contribution in year 2300 of each extreme scenario to the scenario without extremes(MIROC5) for the full dynamic simulations.

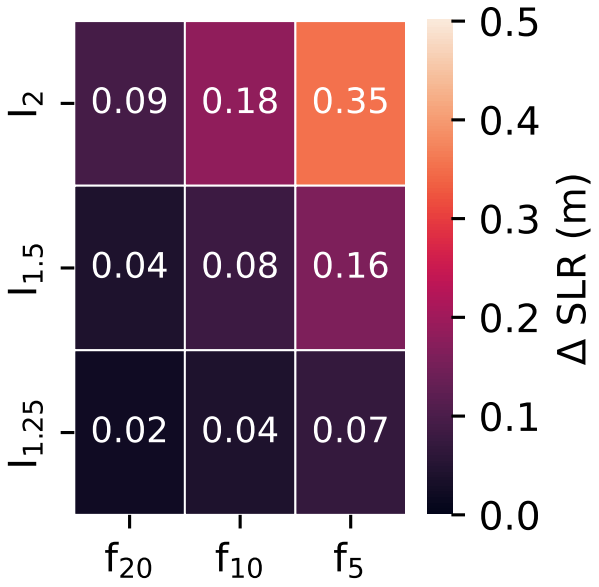

Fig. S28. Importance of intensity and frequency of extremes for the dynamic simulation without surface elevation feedback. Given is the projected sea-level rise contribution in year 2300 for the SMB-only case, for each extreme scenario, subtracted by the sea-level rise scenario without extremes (MIROC5) in 2300 (see also Table 2).

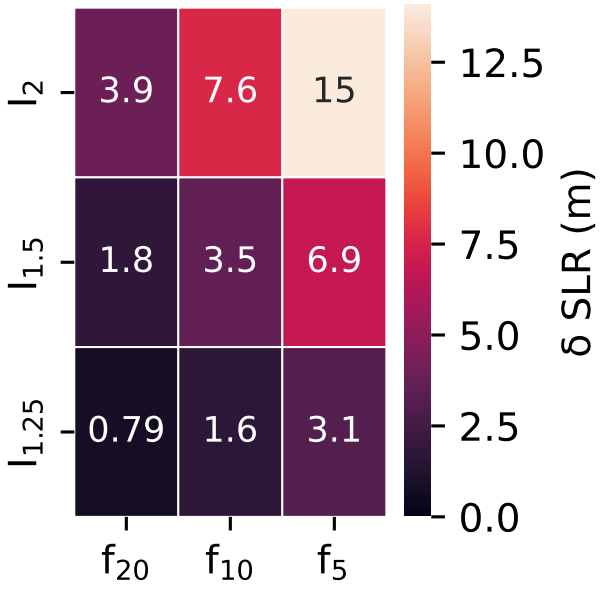

Fig. S29. Relative importance of intensity and frequency of extremes for the dynamic simulation without surface elevation feedback. Given is the relative increase of the projected sea-level rise contribution in year 2300 of each extreme scenario to the scenario without extremes(MIROC5) for the full dynamic simulations.

References

Delhasse, A., Fettweis, X., Kittel, C., Amory, C., and Agosta, C.: Brief communication: Impact of the recent atmospheric circulation change in summer on the future surface mass balance of the Greenland Ice Sheet, Cryosphere, 12, 3409–3418, https://doi.org/10.5194/tc-12-3409-2018, 2018.

IMBIE2016: Rignot Drainage Basins, http://imbie.org/imbie-2016/drainage-basins/GRE_Basins_IMBIE2_v1.3 (2019), 2019.

Joughin, I., Smith, B. E., and Howat, I. M.: A complete map of Greenland ice velocity derived from satellite data collected over 20 years, Journal of Glaciology, 64, 1–11, https://doi.org/10.1017/jog.2017.73, 2018.

Morlighem, M.: IceBridge BedMachine Greenland, Version 3, https://nsidc.org/data/idbmg4/versions/3(2019), 2019.

Morlighem, M., Williams, C. N., Rignot, E., An, L., Arndt, J. E., Bamber, J. L., Catania, G., Chauché, N., Dowdeswell, J. A., Dorschel, B., Fenty, I., Hogan, K., Howat, I., Hubbard, A., Jakobsson, M., Jordan, T. M., Kjeldsen, K. K., Millan, R., Mayer, L., Mouginot, J., Noël, B. P., O'Cofaigh, C., Palmer, S., Rysgaard, S., Seroussi, H., Siegert, M. J., Slabon, P., Straneo, F., van den Broeke, M. R., Weinrebe, W., Wood, M., and Zinglersen, K. B.: BedMachine v3: Complete Bed Topography and Ocean Bathymetry Mapping of Greenland From Multibeam Echo Sounding Combined With Mass Conservation, https://doi.org/10.1002/2017GL074954, 2017.

Mouginot, J., Rignot, E., Bjørk, A. A., van den Broeke, M., Millan, R., Morlighem, M., Noël, B., Scheuchl, B., and Wood, M.: Forty-six years of Greenland Ice Sheet mass balance from 1972 to 2018, Proceedings of the National Academy of Sciences of the United States of America, 116, 9239–9244, https://doi.org/10.1073/pnas.1904242116, 2019.

Palmer, M. D., Harris, G. R., and Gregory, J. M.: Extending CMIP5 projections of global mean temperature change and sea level rise due to thermal expansion using a physically-based emulator, Environmental Research Letters, 13, https://doi.org/10.1088/1748-9326/aad2e4, 2018.

Rignot, E. and Mouginot, J.: Ice flow in Greenland for the International Polar Year 2008-2009, Geophysical Research Letters, 39, 1–7, https://doi.org/10.1029/2012GL051634, 2012.